Transactions, SMiRT-23
Manchester, United Kingdom - August 10-14, 2015
Division V, Paper ID 759

BUCKLING BEHAVIOUR OF SPENT NUCLEAR FUEL RODS

Uma Ramasamy[1], Luis F. Ibarra[2] and Ricardo A. Medina[3]

[1] Post Doctorate Scholar, University of Utah, US
[2] Assistant Professor, University of Utah, US
[3]Associate Professor, University of New Hampshire, US

ABSTRACT

This study assesses the mechanical performance of spent nuclear fuel (SNF) rods when subjected to impact loading due to transportation accident scenarios after long-term storage. The fuel rod consists of a zircaloy cladding that stores fuel pellets. The SNF rod buckling performance is largely affected by pellet-cladding interaction (PCI) caused by exposure to high temperatures and irradiation. Numerical models were created in finite element software to evaluate the linear and nonlinear buckling capacity of 533 mm (21 in.) SNF rod segment, a typical unsupported length between spacer grids. Numerical simulations were carried out for the following fuel rod configurations: i) pellet-cladding gap of 80 μm, and pellet-pellet in contact; ii) PCI and pellet-pellet in contact; and iii) PCI and pellet-pellet bonded. Geometric imperfections were included in buckling capacity analyses to account for initial imperfections and creep deflection after long term storage. Although creep is more likely to occur during early storage, it is considered in the analyses because it leads to fuel rod imperfections that affect buckling capacity. The results indicate that buckling capacity of fuel rods increases when PCI is taken into account, and decreases as initial imperfections increase. Post-buckling behavior of the 533 mm (21 in.) section of SNF rods exhibited elastic buckling due to the relatively large slenderness ratio.

INTRODUCTION

Spent nuclear fuel (SNF) rods in nuclear power plants (NPPs) are first transferred from the reactor to pools for several years, and then to dry cask storage at sites contiguous to plants, known as interim spent fuel storage installations (ISFSIs). Initially, ISFSIs were licensed for 20-year periods, and thereafter SNF should be transported to disposal sites. Nowadays, however, operating ISFSI compliance periods of hundreds of years are being considered. Thus, aging effects need to be part of SNF rod mechanical evaluation under potential accident scenarios during transport operations, given that this deterioration reduces material fracture toughness and yield strength mechanical properties (Rigby and Kadak, 2010). Accident scenarios during transportation can lead to impact loads on SNF rods. Under these impact compression loads, SNF rods are susceptible to breach in an end on impact due to buckling failure (Biglin and Resnikoff, 2006).

Buckling mechanisms cause the elements to deflect laterally and fail by bending. The buckling load, or bifurcation point, is the critical load or stage between stable and unstable condition of a structure, whereas the buckled mode shapes are the characteristic shape associated with the buckled response (Gere, 2013). Eigenvalue buckling analyses based on Euler's formulation accurately predict the buckling capacity of components with uniform cross section. For SNF rods, however, nonlinear buckling analysis is needed because the rod's cross section is not a uniform composite structure. That is, the cladding-pellet and pellet-pellet gaps lead to geometric nonlinearities that cannot be addressed using classical Euler's formulation.

In the early stages of irradiation, the fuel material is densified. This densification is followed by swelling due to the accumulation of solid fission products within the material. Meanwhile, the cladding is subjected to high temperatures (about 350 C) and creeps down because of compressive stresses due to water pressure (7 – 15 MPa). After a few reactor operating cycles, the fuel rod cladding fits the pellet shape and adopts a

bamboo-ridge shape (Marchal et al., 2009). Also, the pellet-cladding gap tends to close once the fuel rod is irradiated and subjected to high temperatures in the reactor. The fuel rod performance is expected to be largely affected by this pellet-cladding interaction (PCI).

Previous studies have addressed fuel rods buckling capacity, but including simplifications for PCI in their "g" load calculation. For instance, Sanders et al. (1992) used only the percentage of fuel pellet mass effective in loading the cladding. They considered that roughly 75% of the fuel pellet mass was attached to the cladding in pressurized water reactors (PWRs). For boiling water reactors (BWRs) the effective pellet mass attached to the cladding was assumed as 10%. These assumptions are based on evidence of BWR SNFs showing minimal PCI, whereas in PWR model fuel pellets are sufficiently attached to the cladding. Based on the assumed percentage of fuel pellet mass attached to cladding, the number of "g's" required to cause buckling of the cladding was calculated. Ramsey et al. (1987) only considered the weight of cladding and neglected the weight of fuel pellets in their analytical calculation for "g" load necessary for axial buckling. In addition, Bjorkman (2010) concluded that the impact "g" load magnitude of a fuel rod under inertia loading depends on the weight of the cladding and fuel rod, regardless of whether the fuel is bonded to the cladding.

This study evaluates the influence of PCI on the buckling capacity and post-buckling behaviour of SNF rods considering initial rod imperfections caused by creep mechanisms. The study presents numerical simulations with intact cladding and fuel rod components for the following configurations: i) pellet-cladding gap, and pellet-pellet in contact; ii) PCI and pellet-pellet in contact; and iii) PCI and pellet-pellet bonded. Case 1 may be expected to occur in BWRs, whereas Case 2 is more likely to take place in PWRs. Case 3 is unlikely to occur because a strong pellet-pellet bond is not usually developed, but it provides an upper bound for the fuel rod behaviour. The scope of this study is limited to deflection on the rods caused by creep mechanisms. Although creep is more relevant during early storage, it is considered in the analyses because it leads to fuel rod imperfections that affect buckling capacity.

FINITE ELEMENT MODEL DESCRIPTION

SNF rods are placed in fuel assemblies that provide lateral support at the grid spacer's location. Depending on the fuel assembly configuration, the most common SNF rod lengths vary from 3200 mm (126 in.) to 3861 mm (152 in.), and the grid spacer supports are usually located from 381 mm to 635 mm (15 to 25 in.), except at the end of the rods, which may have unsupported lengths of 51 – 76 mm (2-3 in.) (DOE, 1987). In this study, the evaluated fuel rod has an unsupported length of 21 in., corresponding to the most common length between grid spacers in a Westinghouse W17 × 17 fuel assembly.

Table 1: Dimensions of fuel rod

Dimension	**Value (mm)**
Length of clad	532.00
Outer diameter of clad	10.54
Clad thickness	0.60
Clad inner diameter	9.34
Length of pellet	14.00
Pellet diameter	9.18

The initial fuel rod configuration consists of uranium dioxide pellets inserted into a cladding tube with a small gap between them. A gap of about 80 – 100 microns (μm) exists initially between the pellet and the clad. The pellet and clad dimensions were obtained from the INL/CON-09-15677 report (Williamson and

Knoll, 2009), and are presented in Table 1. The fuel pellets are modeled as cylinders with top and bottom flat surfaces, and aligned with the same centroidal axis as the cladding (Figure 1).

Finite Element (FE) Mesh

The model was created in the multi-purpose software Abaqus (Abaqus V6.14). The mesh shown in Figure 1 was generated with C3D8R elements (solid reduced integration linear brick elements) for fuel pellets, and C3D8I (solid linear continuum shell elements) for the cladding. The C3D8I elements are appropriate to characterize bending behaviour, even when only one element is utilized through the cladding thickness (Brown, 1997), whereas the C3D8R element with a relatively coarser mesh can be selected for complex structures involving mechanical interactions (Zhan and Li, 2013). Alternative elements were considered, such as the shell S4R element (linear quadrilateral shell element) for the cladding, but its use caused element penetration between pellet and cladding when using surface-to-surface contact and general contact options. A tie constraint was used to simulate the bonded condition between pellet and cladding, and pellet-to-pellet. The effectiveness of the tie constraint was evaluated in Abaqus by comparing a model of three 14 mm (0.55 in.) pellets with tie constraint to an equivalent one-single pellet of 42 mm (1.65 in.). A comparison of Von Mises (VM) stresses, displacements, and contact pressures of the two models resulted in differences smaller than 3%. Therefore, an all-bonded condition was simulated using tie constraints with position tolerance of 0.1 mm, a tolerance larger than the 80 μm pellet-cladding gap.

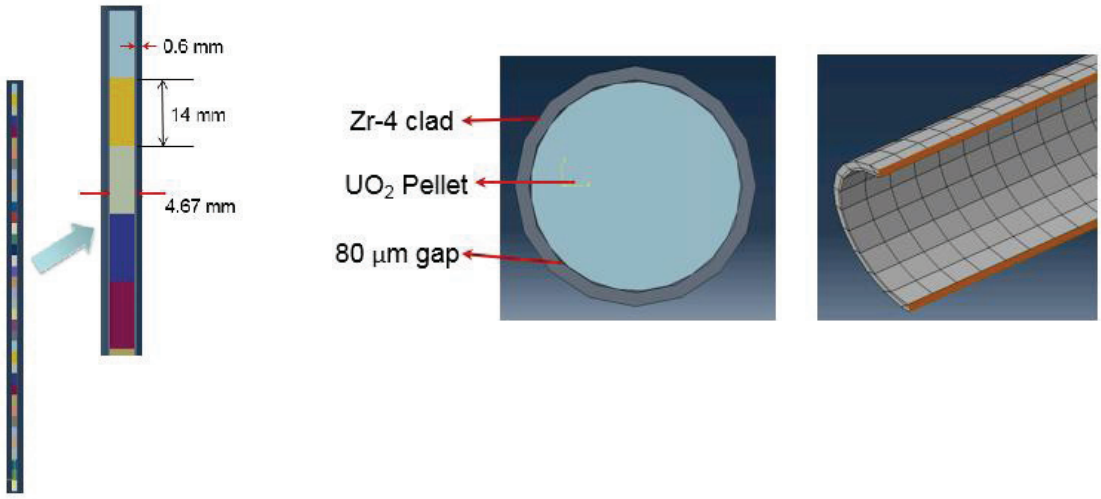

Figure 1. Dimensions of fuel rod (a) elevation (b) cross section

Material properties

The outer cladding of the evaluated SNF is made of Zircoly-4 (DOE, 1987), whereas the fuel pellets are uranium dioxide, UO_2. Material properties used in FE model components for UO_2 (Table 2) are based on FCRD-UFD-2013-000325 report (Adkins et al., 2013). A true stress - plastic strain curve of unirradiated Zr-4 was used in the FE model, which is calculated from engineering stress strain data shown in Figure 2 (Matweb, 2015), as follows.

$$\epsilon_{true} = \int_{L_0}^{L} \frac{dL}{L} = ln\,(1 + \epsilon_{nom}) \tag{1}$$

The true strain can also be expressed in terms of area change (Drucker, 1967)

$$\epsilon_{true} = \ln\left(\frac{A_0}{A_{min}}\right) \tag{2}$$

And from Eqns. (1) and (2), the true stress is

$$\sigma_{true} = \sigma_{nom}\,(1 + \epsilon_{nom}) \tag{3}$$

The plastic strain is obtained as

$$\epsilon_{pl} = \left(\epsilon_{true} - \frac{\sigma_{true}}{E}\right) \tag{4}$$

In the above equations, ϵ_{true} and σ_{true} are the true strain and stress, respectively; whereas ϵ_{nom} and σ_{nom} are the nominal strain and stress. Also, L_0 and A_0 are the initial length and area, respectively.

Table 2: Material Properties of Fuel Rod

Properties	**Zr-4**	**Uranium Dioxide**
Young's Modulus, E (N/mm^2)	99,300	166,000
Poisson's ratio, μ	0.37	0.21
Density (tonne/mm^3)	6.59E-09	1.03E-08

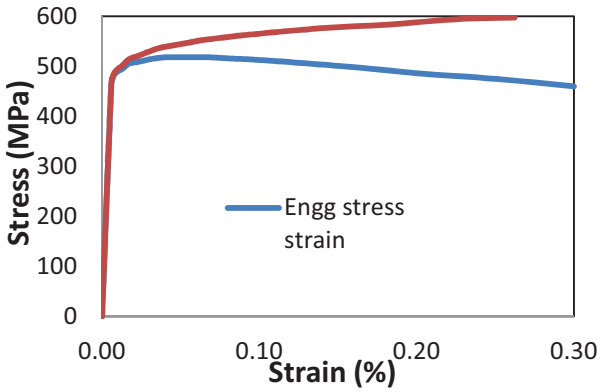

Figure 2. Stress-strain curve of unirradiated Zr-4 cladding

Boundary Conditions and Interactions

The bottom end of the fuel rod is pin-connected to allow free rotation. The top end boundary condition allows free rotation, and it is free to translate in the direction parallel to the longitudinal axis of the rod. The pin condition is a model simplification because the grid spacers actually allow limited lateral displacement between rod and spacer boundary. To implement these boundary conditions in Abaqus, a reference point RP1 was defined at the cladding bottom surface that prevents translation, but allows rotation in X, Y and Z directions. At the top end, reference points RP2 and RP3 were defined at the cladding top and pellet top surface, respectively. RP2 and RP3 were restrained to prevent translation in the X and Y lateral directions, and to allow fuel rod longitudinal displacements in the Z-direction. Coupling constraints were applied

(Figure 3) between the reference points and end cross sections of fuel rod to which the reference points are attached. A coupling constraint couples the action between a point and surface, without adding rotational restraint to a surface. The bottom end of fuel rod is closed with a circular lid, whereas the top end is open. The fuel pellets were only constrained by direct contact with the cladding components at the bottom surface.

The dynamic impact loading is represented in these models as an equivalent static load based on the inertial forces generated by the fuel rod mass (cladding and pellets). This mass includes the self-weight of the modelled SNF rod segment, as well as the weight of the pellets and cladding above this segment. Load demands were estimated to compare them to the computed buckling load capacity. For the buckling load analysis, the mass is distributed according to the mass fraction of the fuel rod components. Thus, the pellet takes 85% and cladding 15% of total buckling load.

General contact interaction was used for surfaces that may be in contact, but not bonded. This contact was used to enforce pellet-to-pellet and pellet-to-clad interaction using a friction coefficient of 0.25 (Williamson and Knoll, 2009). General contact can accurately represent uniform contact tractions irrespective of mesh details (Harkness, 2009). It uses surface geometry corrections to mitigate errors associated with faceted representation of curved surface (NAFEMS, 2009). Robustness, accuracy, performance and scalability of general contact is as good or better than using surface contact interactions, but with extra contact tracking time (King et al. 2013). In this study, the general contact interaction approach provided more stable results than surface-to-surface contact, irrespective of mesh size and stress variation.

LINEAR EIGENVALUE BUCKLING ANALYSIS

The SNF rod buckling was evaluated based on i) linear eigenvalue buckling analyses using linear perturbation procedure, and ii) nonlinear buckling analysis using the Riks method. To study PCI effect on buckling capacity, both methods consider the following numerical simulations of 21-in. fuel rods on intact cladding and fuel rod components

1) Pellet-cladding gap of 80 μm and pellet-pellet in contact
2) Pellet-cladding interaction (PCI) and pellet-pellet in contact
3) PCI and pellet-pellet bonded

The analytical Euler buckling load P_{cr} for the Case 3 SNF rods can be computed as

$$P_{cr} = \frac{\pi^2 EI}{(KL)^2} \tag{5}$$

Where I is moment of inertia about the buckling axis, K is the effective length factor based on end boundary conditions (e.g., for pinned end conditions, K = 1). The Euler buckling load for the 532 mm-fuel road was calculated as 2,887 N according to Equation 5, which is 0.9 % higher than the numerical simulation prediction for linear analysis of Case 3 (Table 3). For which the moment of inertia, I, is calculated assuming PCI, complete bonding between pellet, and in perfect alignment (i.e., same centroidal axis for all pellets and cladding). Based on the SNF rod WE 17 × 17 self-weight (24.43 N/fuel rod), an impact deceleration of 118 g is required to exceed the Euler buckling capacity of 2,887 N. As a comparison, Ramsey et al. (1987) reported a deceleration of 82 g at initial storage for end drop tests of storage casks. To prevent damage to the fuel rods, Ramsey et al. recommended a deceleration limit of 82 g at initial storage, and 95 g for rods after twenty years of storage, as modulus of elasticity increases when temperature reduces at later age.

The FEM buckling capacity of Case 3 was higher compared to Cases 1 and 2 (Table 3), an expected result because of the PCI, and pellet-pellet composite action. The FEM results of linear eigenvalue analysis

showed this interaction influences the buckling capacity, as Case 2 and 3 buckling capacity was 9 and 12% times larger than that of Case 1, respectively. Note that buckling load of Case 3 is only 3% larger than that of Case 2, which indicates that the influence of pellet-pellet bonding on buckling capacity is less relevant than PCI.

A lower bound buckling capacity of the cladding is established by considering only the stiffness contribution of the cladding, and disregarding the stiffness provided by the pellets. In this case, the buckling load is 798 N, according to Equation 5. This buckling load of cladding alone is significantly smaller than that expected for cladding with pellets.

Table 3: Buckling Capacity of 21 in. fuel rod from Eigen Value Analysis

Configuration	Buckling capacity (N)	Capacity as function of "g"
Case 1	2546	104
Case 2	2774	114
Case 3	2862	117
Clad only	771	32

RIKS NONLINEAR BUCKLING ANALYSIS

Method Description

The Riks method can be used to predict unstable, geometric nonlinear instability of a structure with linear and nonlinear materials (Novoselac et al., 2013). The modified Riks nonlinear method included in Abaqus was used to evaluate the SNF rod post-buckling behavior. Riks analyses are needed because of the SNF rod geometric non-linearity caused by the gap between cladding and pellets, and pellet-pellet contacts. These conditions may lead to an unstable post buckling response, in which load and displacement may decrease as the solution evolves. The Riks method uses the load magnitude as an additional unknown, and it solves simultaneously for loads and displacements. The analysis necessitates the incorporation of either geometric or loading imperfections. Geometric imperfections are introduced by perturbations in the geometry and can be defined in three ways: i) As a linear superposition of buckling eigenmodes, ii) as displacements from a previous static analysis, or iii) by direct implementation of initial displacement values at selected nodes..

Effect of initial imperfections on buckling capacity

A geometric imperfection was introduced as a parabolic deflection profile with deflections of 0.1, 0.5, 1.0 and 2.0 mm at the mid length of fuel rod (i.e., 0.02, 0.1, 0.2, and 0.4% of the unsupported length of the rod). These imperfections are applied to both cladding and pellets keeping the same gaps at any given cross-section. The smaller deflections may be caused by initial geometric imperfections, whereas larger deflections may account for creep mechanisms after long term storage. The maximum values were selected by considering that the fuel rod pitch, or gap between outer diameter of contiguous fuel rods, is 3.6 mm. A maximum displacement of 20 mm (4% of the initial unsupported length) was specified in the lateral direction at middle of rod (in center node of the pellet) to stop the Riks analysis. Note that although the gap between contiguous rods is less than 4 mm, the lateral displacement may be much larger, as it is possible for adjacent fuel rods to buckle in the same direction.

Figures 5-7 present SNF axial load-displacement curves for Cases 1, 2, and 3. The displacements are monitored at the center node pellet (CNP) in the fuel rod lateral direction 1. For the three cases, elastic buckling controls SNF rod instability because of their large slenderness ratio. For example, for Case 3 in

which the cladding and pellets are acting in composite action, the slenderness ratio KL/r = 143. This ratio is associated with a fuel rod plastic stress σ = 73 MPa, according to Equation 5, which is higher than the Von Mises stress at critical buckling load of Case 1, σ_{VM} = 67 MPa obtained from FEA analysis, shown in Figure 8. Therefore, 532 mm (21-in.) fuel rods are expected to fail due to elastic instability before its yield strength is reached, indicating that elastic and inelastic analyses provide the same buckling load capacity. This fact was verified for the three 532 mm (21-in.) fuel rod cases with initial imperfections including 0.1mm, 0.5mm, 1mm, 2mm and 5mm. Load displacement curves of the three cases overlapped one another when linear and nonlinear material properties were used.

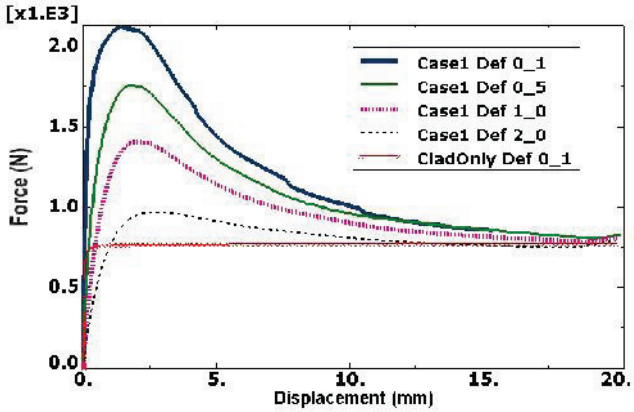

Figure 5. CASE1 Riks Analysis - Load-displacement plot of center node pellet in "X" lateral direction with 0.1, 0.5, 1.0 and 2.0 mm imperfection.

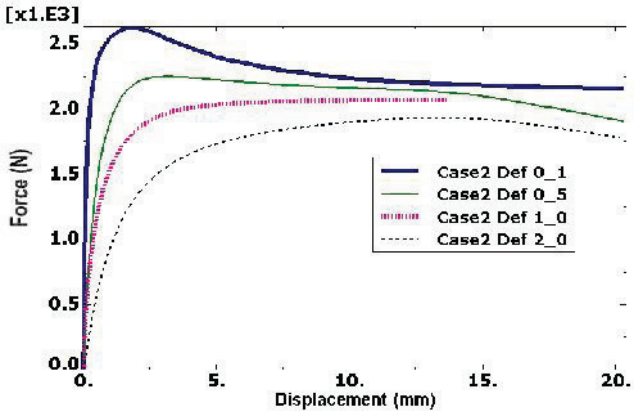

Figure 6. CASE2 Riks Analysis - Load-displacement plot of center node pellet in "X" lateral direction with 0.1, 0.5, 1.0 and 2.0 mm imperfection.

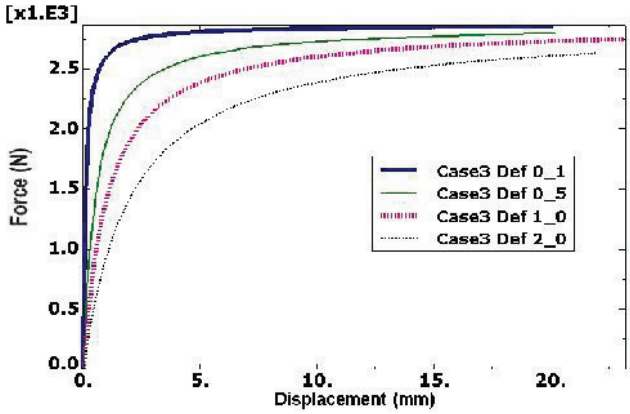

Figure 7. CASE3 Riks Analysis - Load-displacement plot of center node pellet in "X" lateral direction with 0.1, 0.5, 1.0 and 2.0 mm imperfection.

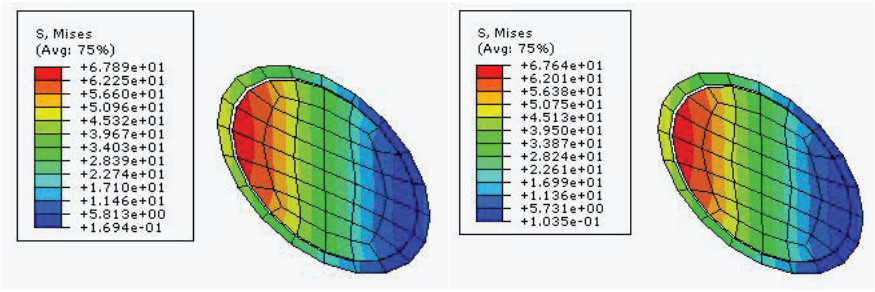

(a) (b)

Figure 8. Von Mises stresses plot of Case 1 at middle section of fuel rod. (a) elastic material analysis, (b) inelastic material analysis

Riks realizations with different initial imperfections for Case 1 SNF showed a significant strength decrease after the bifurcation point. The buckling capacity is larger for small initial imperfections, and the strength reduction more pronounced. For instance, for an initial imperfection of 0.1 mm, P_{cr} = 2,125 N at the bifurcation point, but at a lateral mid displacement of 20 mm, this load approaches 800 N. The strength of the clad-only case is 771 N in Table 3. For SNF rods with larger initial imperfections the buckling load is smaller, and strength reduction is less pronounced, because the initial benefit of a small pellet-cladding clearance is partially offset by the large imperfection. As observed in Figure 5, the post buckling strength of Case 1 curves for different imperfections eventually converge to a load of 800 N, which is the buckling capacity of cladding only. This behavior indicates that as the post-buckling transverse displacement increases, the initial contribution from pellet-to-pellet and pellet-to-cladding interaction decreases, until it becomes negligible at large deformations.

For Case 2, the post-buckling behavior shows a strength decrease after the bifurcation point when the imperfection is 0.1 and 0.5 mm. Larger initial imperfections do not lead to strength reduction because the initial PCI beneficial effect diminished due to the large initial imperfections. The bifurcation point shows an increase of approximately 20% with respect to Case 1, as a result of perfect bond between pellets and cladding. The largest benefit of PCI is the larger ultimate post-buckling load of 2,000 N. This value is an increase of more than 100% with respect to Case 1 with 0.1 mm imperfection. The post-buckling behavior of Case 3 does not show a strength reduction because the pellet-to-pellet and pellet-to-cladding bonding makes the fuel rod behave as a solid composite rod, eliminating initial geometric nonlinearities. As shown in the Figure 9, the major benefit of a pellet-pellet bond would be a stable post-buckling behavior.

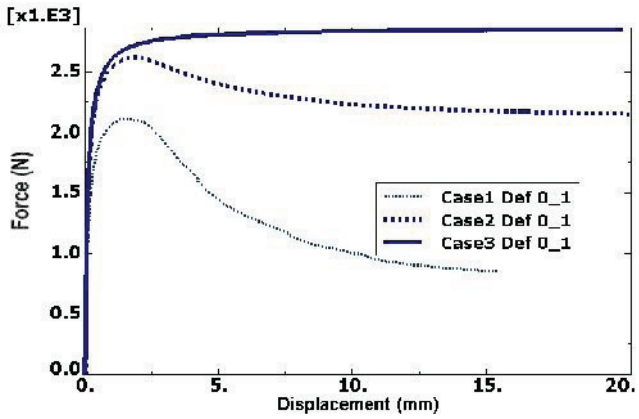

Figure 9. Load-displacement plot of center node pellet in X direction for Imperfection 0.1 mm

Table 4 shows the buckling load and Von Misses stresses from geometric nonlinear analyses that account for inelastic material properties. The computed buckling capacity of Cases 2 and 3 was 20 and 30% larger than that of Case 1. However, all stresses are below the yield strength value of 381 MPa.

Table 4. Buckling Capacity and Maximum Von Mises Stress of 21 in. fuel rod with Inelastic Material Properties and 0.1 mm imperfection

Configuration	Buckling Load (N)	Max VM Stresses (MPa)
Case 1	2,173	69
Case 2	2,624	77
Case 3	2,769	80

CONCLUSIONS

The buckling behaviour of SNF rods was numerically evaluated to assess the influence of pellet-cladding interaction (PCI) and pellet-pellet friction contact in the presence of initial imperfections and creep-induced deflections. Numerical simulations were carried out with intact cladding and fuel rod components for the following configurations: i) pellet-cladding gap and pellet-pellet in contact; ii) PCI and pellet-pellet in contact; and iii) PCI and pellet-pellet bonded. These models were used to determine the effect of bonding on buckling capacity of intact axially loaded fuel rods, as well as rod's post-buckling behaviour. Geometric imperfections were introduced to account for initial imperfections and creep deflection after long term storage. Although creep is more likely to occur during early storage, its effects may affect buckling capacity after extended periods of time.

The results from this numerical study demonstrate that the buckling capacity of a 21-in. fuel road is controlled by elastic buckling. This implies that accurate characterization of fuel-rod material degradation mechanisms, when ductile behaviour controls the material response, might not be critical to evaluate deceleration limits associated with accident scenarios. The effect of material degradation mechanisms that could significantly impair the fracture toughness of the cladding needs to be investigated.

In addition, the presence of PCI increases (a) the fuel-rod buckling capacity when small initial imperfections are present (e.g., a 20% increase for a 0.1 mm initial imperfection), and (b) the post-buckling residual strength at large deflections when pellets are in contact with one another (e.g., 2,500 N *vs* 800 N when PCI is included with an initial imperfection of 0.1mm). The best behaviour is obtained when PCI is modelled

and the pellets are bonded, for a decrease in buckling load capacity is not observed as the lateral deformation increases.

When PCI is neglected and small initial imperfections are present (1mm or less), the relatively small clearance between the pellets and cladding produces an increase of a factor of approximately three in the buckling capacity with respect to the clad-only condition. If creep-induced deflections in the order of 10 mm or more are present and PCI is ignored, the buckling capacity is expected to be controlled by the cladding. Thus, for conditions in which PCI is significant after long-term storage, ignoring this effect could significantly underestimate deceleration limits for accident scenarios.

ACKNOLEDGEMENTS

Authors would like to thank US DOE for funding the project DE-NE0000698 001. Also, authors thank the consultant of this project, Justin Coleman, from Idaho National Laboratory for his valuable inputs.

REFERENCES

ABAQUS/Explicit Version 6.14 (2014) ABAQUS, Inc.

Adkins, H., Geelhood, K., Koeppel, B., Coleman, J., Bignell, J., Flores, .G., Wang, J-A., Sanborn, S., Spears R.., Klymyshyn, N. (2013). "Used Nuclear Fuel Loading and Structural Performance Under Normal Conditions of Transport-Modeling, Simulation and Experimental Integration RD&D Plan," *Used Fuel Disposition Campaign*, FCRD-UFD-2013-000135, U.S. DOE.

Bjorkman, G. S., (2010). "The Buckling of Fuel Rods under Inertia Loading," *Spent Fuel Transportation Division*, U.S. NRC.

Brown, J., (1997). "Characterization of MSC/NASTRAN & MSC/ABAQUS Elements for Turbine Engine Blade Frequency Analysis," *MSC Aerospace Users Conference Proceedings*.

Drucker, D. C., (1967). "Introduction to Mechanics of Deformable Solids," McGraw Hill, Inc., NY.

Gere, J., and Goodno, B. (2013). "Mechanics of Materials." Eighth edition, Cengage learning, USA.

Harkness, H., and Ang, G. (2009). "General contact for Implicit FEM", *Proceedings of NAFEMS World Congress*.

http://www.matweb.com/ATI WahChangZirconiumAlloyZircaloy-4.

King, S., Richards, T., (2013). "Solving Contact Problems with Abaqus", http://moodle.insa-toulouse.fr/pluginfile.php/42654/mod_resource/content/3/CONTACT_Imulia.pdf, Accessed 10/14

Marchal, M, Campos, C., and Garnier. (2009). "Finite element simulation of Pellet-Cladding Interaction (PCI) in nuclear fuel rods," *Computational Materials Science* 45, 821–826.

Novoselac, S., Ergic, T, and Balicevic, P. (2012). "Linear and Nonlinear Buckling and Post Buckling Analysis of a Bar with the Influence of Imperfection," *Technical Gazette*, Vol.19, pp. 695-701.

Ramsey, C., Monika, W., Schwartz, M., (1987). "Dynamic Impact Effects on Spent Fuel Assemblies," *UCID21246*, Lawrence Livermore National Laboratory, Livermore, California.

Rigby, D. B., Kadak, A. (2010) "Evaluation of the Technical Basis for Extended Dry Storage and Transportation of Used Nuclear Fuel," *United States Nuclear Waste Technical Review Board.*

Sanders, T., Seager, K., Rashid, Y., Barrett, P., Malinauskas, A., Einziger, R., Jordan, H., Duffey, T., Sutherland, S., Reardon, P., (1992). "A Method for Determining the Spent Fuel Contribution to Transport Cask Containment Requirements," *SAND90-2406*, Sandia National Laboratories, NM.

U.S. DOE (1987). "Characteristics of spent fuel, high level waste, and other radioactive wastes which may require long term isolation," *Appendix 2 A Physical description of LWR Fuel Assemblies.*

Williamson, R., Knoll, D. (2009). "Enhancing the ABAQUS Thermomechanics Code to Simulate Steady and Transient Fuel Rod Behavior," *Proceedings of Top Fuel*, Paper 2072, 2009.

Zhan, Y., and Li, M. (2013). "A Comparative Study on Numerical Buckling Analysis for a Cantilever Steel Pipe Column under Combined Loads," *International Journal of Engineering Research*, V.2 Issue 3. pp 253-256.